METHYLENE BLUE ADSORPTION ON THE BASAL SURFACES OF KAOLINITE: STRUCTURE AND THERMODYNAMICS FROM QUANTUM AND CLASSICAL MOLECULAR SIMULATION

JEFFERY A. GREATHOUSE[1],*, DAWN L. GEATCHES[2], DARIN Q. PIKE[3], H. CHRISTOPHER GREENWELL[4], CLIFF T. JOHNSTON[5], JENNIFER WILCOX[2], AND RANDALL T. CYGAN[1]

[1] Geochemistry Department, Sandia National Laboratories, P.O. Box 5800, MS 0754, Albuquerque, NM 87185-0754, USA
[2] Energy Resources Engineering, Earth Sciences, Stanford University, CA 94305-2220, USA
[3] Chemical and Biological Systems Department, Sandia National Laboratories, P.O. Box 5800, MS 0734, Albuquerque, NM 87185-0734, USA
[4] Department of Earth Sciences, Durham University, South Road, Durham DH1 3LE, UK
[5] Crop, Soil, and Environmental Sciences, Purdue University, West Lafayette, IN, 47097, USA

Abstract—Organic dyes such as methylene blue (MB) are often used in the characterization of clays and related minerals, but details of the adsorption mechanisms of such dyes are only partially understood from spectroscopic data, which indicate the presence of monomers, dimers, and higher aggregates for varying mineral surfaces. A combination of quantum (density functional theory) and classical molecular simulation methods was used to provide molecular detail of such adsorption processes, specifically the adsorption of MB onto kaolinite basal surfaces. Slab models with vacuum-terminated surfaces were used to obtain detailed structural properties and binding energies at both levels of theory, while classical molecular dynamics simulations of aqueous pores were used to characterize MB adsorption at infinite dilution and at higher concentration in which MB dimers and one-dimensional chains formed. Results for the neutral MB molecules are compared with those for the corresponding cation. Simulations of the aqueous pore indicate preferred adsorption on the hydrophobic siloxane surface, while charge-balancing chloride ions adsorb at the aluminol surface. At infinite dilution and in the gas-phase models, MB adsorbs with its primary molecular plane parallel to the siloxane surface to enhance hydrophobic interactions. Sandwiched dimers and chains are oriented perpendicular to the surface to facilitate the strong hydrophobic intermolecular interactions. Compared with quantum results, the hybrid force field predicts a weaker MB adsorption energy but a stronger dimerization energy. The structure and energetics of adsorbed MB at infinite dilution are consistent with the gas-phase binding results, which indicate that monomer adsorption is driven by strong interfacial forces rather than by the hydration properties of the dye. These results inform spectroscopic studies of MB adsorption on mineral surfaces while also revealing critical areas for development of improved hybrid force fields.

Key Words—Adsorption, Kaolinite, Methylene Blue, Organic Dye.

INTRODUCTION

In addition to numerous applications in biology and medicine (Wainwright, 2000; Wainwright and Crossley, 2002; Oz *et al.*, 2011), organic dyes have long been used to determine surface properties of hydrated clays and soils (Hang and Brindley, 1970; Maček *et al.*, 2013; Heister, 2014). Cationic dye molecules can undergo ion exchange at permanent charge sites on internal and external surfaces, as well as at acid sites on mineral edges (Cenens and Schoonheydt, 1988). Once adsorbed, spectrophotometric properties of the dye molecule allow its local structure to be probed by, for example, ultraviolet and visible (UV-Vis) spectroscopy (Lagaly *et al.*, 2013). Changes in the UV-Vis spectrum of the dye can then be investigated as a function of solution conditions (*e.g.* dye concentration, pH), clay layer

charge, and clay morphology revealing monomer adsorption sites as well as dye–dye interactions including the presence of dimers, trimers, and aggregates.

One cationic dye in particular, MB, has been used widely to characterize clay mineral surfaces (Brindley and Thompson, 1970; Hang and Brindley, 1970). Initial UV-Vis spectroscopic results indicated that MB cations (MB$^+$) adsorbed at ion exchange sites on the basal surfaces of smectites, but MB$^+$ dimers, trimers, and higher aggregates formed at higher loadings (Cenens and Schoonheydt, 1988; Schoonheydt and Heughebaert, 1992; Jacobs and Schoonheydt, 1999). This interpretation was later modified by Jacobs and Schoonheydt (2001), however, who noted that UV-Vis peaks due to MB$^+$–MB$^+$ interactions disappeared over time, leaving only the monomer peak. The increase in the monomer peak over time is due to migration of MB$^+$ into interlayer regions after initial adsorption on external smectite surfaces (Neumann *et al.*, 2002). Additionally, the long-term adsorption structure of adsorbed MB$^+$ depends on the strength of the MB$^+$–surface interactions: strong

* E-mail address of corresponding author:
jagreat@sandia.gov

MB$^+$−surface interactions seen at tetrahedral substitution sites (*e.g.* beidellite) result in aggregation of clay particles due to displacement of surface water by MB$^+$, while weak MB$^+$−surface interactions due to octahedral substitution (*e.g.* montmorillonite and hectorite) result in more loosely bound molecules with a blue-shifted UV-Vis peak (Jacobs and Schoonheydt, 2001).

Despite the widespread use of organic dyes to characterize clay minerals and the resulting detailed spectroscopic data, uncertainties remain due to a lack of molecular-level understanding of the adsorption process, including structural details of MB$^+$ aggregates at the surface (Cenens and Schoonheydt, 1988) and the orientation of MB$^+$ relative to the surface (Bujdak *et al.*, 2003). In addition, the in-plane *vs.* out-of-plane pleochroic behavior, based on study of IR bands, to determine molecular orientation was examined by Rytwo *et al.* (1995). Ultimately the presence of strong electrostatic interactions (dye−clay) and hydrophobic interactions (dye−dye) complicates the interpretation of UV-Vis results because the exact location and alignment of adsorbed dye molecules is unknown. This study uses a combination of molecular simulation methods to provide detailed structural and thermodynamic properties of this process. In addition to aiding the interpretation of spectroscopic data of adsorbed dyes, a detailed study of the adsorption properties of organic dyes also provides insight into similar adsorption processes of organic contaminants such as pesticides and pharmaceuticals in the environment.

The electronic, structural, and thermodynamic properties of gas-phase MB$^+$ have been studied using a variety of quantum methods. Hartree-Fock (HF) molecular orbital calculations were used to derive atomic charges for classical simulations (Levy and Enescu, 1998; Enescu *et al.*, 2002), and in other cases density functional theory (DFT) was used to analyze solvent effects on the electronic transitions of MB$^+$ that give rise to its visible spectrum (Quintao *et al.*, 2002; Homem-de-Mello *et al.*, 2005). Atomic charges for MB$^+$ and other dyes obtained from HF and DFT calculations have also been used to assess the ability of these molecules to form hydrogen-bond complexes with lignin (Perdih and Perdih, 2011). The molecular frontier orbitals from DFT calculations were analyzed by Chagovets *et al.* (2012) to investigate MB$^+$ binding to carbon nanotubes.

Modeling the adsorption of MB$^+$ at mineral interfaces often requires larger, more realistic model systems that are still beyond the reach of being tractable by quantum methods. In these cases, classical simulations based on empirically derived force field (FF) parameters yield structural and thermodynamic properties of MB$^+$ and its complexes. Molecular dynamics (MD) simulations have been used to obtain structural properties of ground-state MB$^+$−guanine complexes (Levy and Enescu, 1998) and to investigate solvent rearrangement around the excited state complex to better understand the associated

electron-transfer process (Enescu *et al.*, 2002). Very few FF simulation studies of MB$^+$−clay interactions have been published to date. Yu *et al.* (2000) used MD simulation to show that the orientation of MB$^+$ in smectite interlayers depends on water content, while MB$^+$ adsorbs on external mica surfaces as aggregates with a preferred orientation. More recently, Čapková and coworkers have combined MD simulation and spectroscopic methods to understand the interaction of montmorillonite with molecules of the organic dye rhodamine B (Čapková *et al.*, 2004; Klika *et al.*, 2004) and, more recently, MB (Klika *et al.*, 2007, 2009; Kovar *et al.*, 2009).

Here, classical MD simulations are used to better understand the partitioning of MB$^+$ and Cl$^−$ ions between the hydrophilic and hydrophobic basal surfaces of kaolinite, as well as the tendency of MB$^+$ to aggregate on mineral surfaces at higher concentrations. Additionally, the structural and thermodynamic properties of MB$^+$ adsorption were compared using both quantum and classical methods to evaluate the commonly used approximation of mixing FFs for such hybrid (organic−inorganic) model systems. Other force field approaches have been used for modeling such hybrid systems (Headen and Boek, 2011; Klebow and Meleshyn, 2011; Praus *et al.*, 2011; Rai *et al.*, 2011; Toth *et al.*, 2012; Heinz *et al.*, 2013; Hou *et al.*, 2014; Johnston, 2014), but a detailed comparison of such methods for one specific application is beyond the scope of the present work.

Kaolinite has the general formula Al$_2$Si$_2$O$_5$(OH)$_4$. It is categorized as a 1:1 clay mineral containing sheets of SiO$_4$ tetrahedra and AlO$_2$(OH)$_4$ octahedra. The layer-bounding tetrahedral and octahedral surfaces are referred to hereafter as the siloxane and aluminol surfaces, respectively. Kaolinite is an uncharged and non-swelling clay mineral, so adjacent layers are held together by both hydrogen bonding and dispersion interactions. Kaolinite was chosen to represent neutral siloxane and gibbsite-like Al(OH)$_3$ surfaces that will form a baseline for comparison with charged surfaces (future work). While many of the MB$^+$-clay spectroscopic studies have focused on smectites, similar experiments on kaolinite reveal that MB$^+$ also adsorbs on neutral surfaces (Avena *et al.*, 2001; Ghosh and Bhattacharyya, 2002; Lofaj and Bujdak, 2012).

METHODS

DFT calculations

All DFT electronic structure calculations were performed using the *CASTEP* code (Clark *et al.*, 2005) with a plane wave basis set and pseudopotentials within the DFT formalism (Kohn and Sham, 1965a, 1965b; Payne *et al.*, 1992). The valence electron wave functions were expanded in a plane wave basis set represented by a kinetic energy cut-off of 450 eV, which gave an energy

difference in total energies of <0.2 meV per atom for higher cut-offs. The electron−ion interactions were described by ultrasoft pseudopotentials (Vanderbilt, 1990). These were consistent with the description of the exchange-correlation effects given by the generalized gradient approximation (GGA) density functional, specifically Perdew, Burke and Ernzerhof (PBE) (Perdew *et al.*, 1996). The GGA describes molecular bonding to a greater accuracy than does the local density approximation, and the GGA/PBE approach previously proved itself suitable for study of the adsorption of nitrogen-based organic monomers on kaolinite (Geatches *et al.*, 2012). Dispersive van der Waals forces using the semi-empirical dispersive correction (sedc) model (McNellis *et al.*, 2009) of Grimme (G06) (Grimme, 2006) were included for all DFT systems, primarily as a refinement of the atomic relaxation of the MB molecules. The Broyden-Fletcher-Goldfarb-Shanno (BFGS) (geometry) optimizer (Pfrommer *et al.*, 1997) was used, and the electronic energy minimizer method involved density mixing (Kresse and Furthmuller, 1996).

Other DFT studies found that the B3LYP functional (Becke, 1993) produces a closer match (than the GGA/PBE functional) to experimental vibrational frequencies of aluminosilicates (Demichelis *et al.*, 2010), and to elastic and phase stability properties of mineral systems in general (Wilson and Muscat, 2002), but the computational cost incurred by the B3LYP functional in plane wave codes is prohibitive for the periodic system sizes used here. The combination of GGA/PBE plus dispersion forces was shown to reproduce the experimental structural parameters of sheet silicates including kaolinite to within 1% (Tunega *et al.*, 2012), which, together with the calculation of energy differences in the form of adsorption energies (leading to a cancellation of errors inherent to the DFT methodology) ameliorates the compromise between the choice of exchange-correlation functional, system size, and computational accuracy within this DFT/MD study.

The Brillouin zone integrations were performed at the gamma point for gas-phase molecules and on a Monkhorst Pack (Monkhorst and Pack, 1976) $2 \times 1 \times 1$ grid for the kaolinite and kaolinite/adsorbate systems, as this gave total force convergence to three decimal places. Further convergence details per BFGS iteration are as follows: energy change per ion: dE/ion = 1×10^{-5} eV; electronic energy tolerance: 1×10^{-7} eV; maximum force: $|F|$max = 0.05 eV·Å^{-1}; change in displacement: $|dR|$ = 0.002 Å. All calculations were non-spin polarized and all molecular models were created and visualized using *Materials Studio* (Accelrys, Inc., San Diego, California, USA).

Classical simulations

All interatomic interactions in kaolinite were treated using non-bonded potential energy terms (van der Waals and electrostatic) with parameters taken from *Clayff*

(Cygan *et al.*, 2004). *Clayff* has been shown to reproduce accurately structural, thermodynamic, and dynamical properties of bulk kaolinite (Cygan *et al.*, 2004) and kaolinite interfaces (Croteau *et al.*, 2008, 2009; Tokarsky *et al.*, 2012; Fafard *et al.*, 2013; Haria *et al.*, 2013; Tenney and Cygan, 2014). The energy expression also includes a harmonic bond potential for the hydroxyl group to accurately reproduce O−H distances and vibrations. Parameters for flexible simple point charge (SPC) water and aqueous chloride ions were taken from the literature (Teleman *et al.*, 1987; Smith and Dang, 1994) and are available in *Clayff*. Intramolecular and van der Waals parameters for the MB molecule were taken from the all-atom 'Optimized Potentials for Liquid Simulations' (OPLS) force field (Jorgensen *et al.*, 1984; Jorgensen and Tirado-Rives, 1988), which is well suited to studying the properties of organic molecules and their condensed phases (Jorgensen and Severance, 1990; Jorgensen *et al.*, 1996). Non-bonded parameters for all atoms are given in Table 1.

Atomic charges for MB and MB$^+$ were taken from those obtained by a Mulliken population analysis of the optimized structure of each species from *ab initio* calculations (Enescu *et al.*, 2002). The neutral MB molecule was included to determine the effect of net ionic charge on adsorption. While the reduced (leuco) form of MB is known (MB-H), only the neutral MB molecule was included for consistency with the MB and MB$^+$ charges developed by Enescu *et al.* (2002). The presence of an additional hydrogen atom on MB would also have little impact on the adsorption properties of the molecule. While a Mulliken analysis often underestimates atomic charges, in the present case charges from a minimum basis set reproduce accurately the electrostatic potential obtained using a more advanced basis set (Enescu *et al.*, 2002). Because methyl groups have rotational freedom during MD simulations, charges on these atoms were assigned by averaging explicit charges obtained from the optimized structure (Enescu *et al.*, 2002). Structural properties of the optimized MB$^+$ are in good agreement with the *CHARMM*-based model of Levy and Enescu (1998).

The initial kaolinite structure was taken from Bish (1993). For DFT calculations, a $2 \times 4 \times 1$ supercell was created from the optimized unit cell (Figure 1), and the z dimension of the cell was expanded to create a vacuum-terminated basal (001) surface of kaolinite. The magnitude of the z dimension depended on the type of MB surface complex: 17.0 Å for the MB monomer and 30.0 Å or 34.0 Å for the dimer in parallel or perpendicular orientation, respectively. The use of the smaller vacuum gap is justified based on the small energy difference (~1 meV·atom^{-1}) between optimized kaolinite supercells for z = 17.0 Å and z = 30.0 Å, which is equivalent to the convergence criteria.

The binding energies (E_{BE}) for the DFT simulations were calculated as follows:

Table 1. Non-bonded potential parameters for classical simulations[a].

Atom[b]	q (e)	ε (kcal·mol^{-1})	σ (Å)
Kaolinite (Cygan *et al.*, 2004)			
Al	1.575	$1.330 \cdot 10^{-6}$	4.271
O(H)	−0.950	0.1554	3.166
H(O)	0.425	0	0
Si	2.100	$1.840 \cdot 10^{-6}$	3.302
O	−1.050	0.1554	3.166
Methylene Blue[c]			
S	0.1197 (0.2322)	0.2500	3.550
N1 aromatic	−0.2775 (−0.1742)	0.1700	3.250
N2 amine	−0.2549 (−0.2416)	0.1700	3.250
C1(S)	−0.0755 (−0.0197)	0.0700	3.550
C2(N aromatic)	0.0756 (0.0627)	0.0700	3.550
C3(C2)	−0.0916 (−0.0144)	0.0700	3.550
C4(C3)	−0.1105 (−0.0989)	0.0700	3.550
C5(C4)	0.1152 (0.2094)	0.0700	3.550
C6(C5)	−0.0894 (−0.1173)	0.0700	3.550
H3(C3)	0.0770 (0.1043)	0.3000	2.420
H4(C4)	0.1383 (0.1416)	0.3000	2.420
H6(C6)	−0.0571 (−0.0297)	0.3000	2.420
C7 methyl(N amine)	−0.0644 (−0.0768)	0.0660	3.500
H7 methyl(C methyl)	0.0801 (0.1047)	0.0300	2.500
SPC water (Teleman *et al.*, 1987)			
O(H)	−0.820	0.1554	3.166
H(O)	0.410	0	0
Chloride Ion (Smith and Dang, 1994)			
Cl	−1	0.1001	4.400

[a] Pairwise non-bonded energy terms were calculated using $E_{ij} = q_i q_j/r + 4\varepsilon_{ij}[(\sigma_{ij}/r)^{12} - (\sigma_{ij}/r)^6]$, where E_{ij} is the non-bonded energy between atoms i and j, r is the distance between these atoms, q_i is the charge on atom i and likewise for atom j, $\varepsilon_{ij} = \sqrt{\varepsilon_i \varepsilon_j}$, and $\sigma_{ij} = \sqrt{\sigma_i \sigma_j}$ for the Lennard-Jones well depth (ε) and diameter (σ), respectively.
[b] Atoms are bonded to the atom in parentheses.
[c] Lennard-Jones parameters for MB atoms were taken from the OPLS-AA force field (Jorgensen *et al.*, 1996). Electrostatic charges for MB and MB$^+$ (values in parentheses) were taken from Enescu *et al.* (2002).

$$E_{BE} = E_{slab+ads} - E_{slab} - E_{ads} \qquad (1)$$

where $E_{slab+ads}$ is the energy of the whole system, *e.g.* kaolinite plus neutral MB monomer; E_{slab} and E_{ads} are the energies of kaolinite and the adsorbate, respectively, and the resulting binding energy is negative representing exothermic adsorption. For model systems with two adsorbates (2 MB or 1 MB$^+$ and 1 Cl$^-$), E_{ads} is the sum of isolated gas-phase species rather than the energy of the molecular pair.

For classical minimization and MD simulation, an orthogonalized kaolinite model was expanded into an $8 \times 5 \times 3$ supercell with dimensions $x = 41.5$ Å, $y = 44.6$ Å, and $z = 21.2$ Å. The z dimension was expanded to create either a vacuum-terminated basal surface as described below, or an aqueous pore containing 2548 water molecules with a thickness of ~41 Å. For the gas-phase minimizations, only one kaolinite layer was used for consistency with the DFT model, with a z coordinate of 34.0 Å. Calculations of gas-phase MB monomers and dimers and the chloride ion used an equivalently sized simulation cell but without the kaolinite layer. All minimizations of MB, MB$^+$, or Cl$^-$ adsorbed on the kaolinite surface were carried out under constant volume conditions.

Classical MD simulations were performed for aqueous regions consisting of one or 12 ion pairs (MB$^+$ and Cl$^-$) or 14 neutral MB molecules. For comparison of MB$^+$ hydration properties, MD simulations of aqueous MB$^+$ Cl$^-$ in bulk solution were also performed on a box containing 2548 water molecules and one ion pair. All classical minimizations and MD simulations were conducted with the LAMMPS code (Plimpton *et al.*, 1997) using periodic boundary conditions. A real-space cutoff of 10.0 Å was used for short-range interactions, and long-range electrostatic interactions were calculated with the particle−particle particle−mesh summation algorithm (Plimpton *et al.*, 1997) at a precision of 1.0×10^{-4}.

All MD simulations contained an aqueous region (box or pore) with short-range interactions calculated every 0.5 fs and long-range electrostatic interactions calculated every 1.0 fs. Water molecules were initially
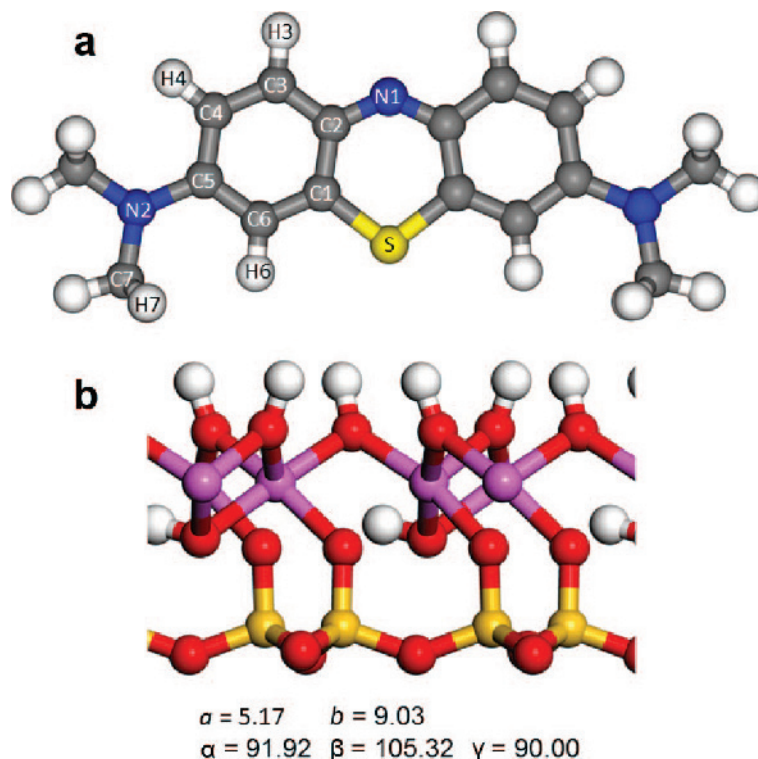
Figure 1. Models of (a) MB$^+$ with FF atom-type labels and (b) the kaolinite unit cell with DFT-optimized dimensions in Ångstroms and degrees. All DFT models contained a vacuum region, so no c-axis value is shown. The atoms are colored as follows: C (gray); N (blue); S (yellow); H (white); O (red); Si (gold); Al (purple).

placed in a crystal lattice and relaxed during a 50 ps *NVE* (microcanonical ensemble) simulation at a temperature of 1000 K, where *N* represents the number of atoms, *V* is the volume, and *E* is the total potential energy. All other atoms (kaolinite and aqueous species) remained fixed at their initial coordinates. Water molecules were then cooled from 1000 K to 300 K during a 50 ps *NVT* (canonical ensemble) simulation, where *T* is the temperature. Next, all atomic motion was allowed during sequential 50 ps *NVE* and *NVT* simulations at 300 K. The supercell thickness was equilibrated and adsorption structures formed during an 11.0 ns *NPT* (isothermal-isobaric ensemble) simulation, where *P* is the pressure which is assigned a value of 0 bar for environmental conditions (note that only the supercell *z* dimension was allowed to change during *NPT* simulation). A final 6.0 ns *NVT* simulation was used to obtain structural properties, with data collected over the final 5.0 ns. During this final *NVT* simulation, four aluminum atoms in the middle kaolinite layer were held at fixed coordinates to avoid drifting of adjacent clay layers. For *NVT* and *NPT* simulations, Nosé-Hoover thermostats and barostats were used with relaxation times of 100 fs and 500 fs, respectively. Using a constant-pressure ensemble ensured that the appropriate water densities at the mineral surface and in the bulk region were maintained (Zeitler *et al.*, 2012).

RESULTS AND DISCUSSION

The DFT calculations of MB adsorption on kaolinite basal surfaces were performed to investigate the structures and energetics of the adsorption process. The DFT results are compared with corresponding classical optimizations in order to assess the quality of the hybrid FF approach used in the present study. Calculations were performed for neutral MB monomers and dimers as well as for MB$^+$ Cl$^-$ ion pairs.

As an initial test of the OPLS-based force field for MB, the dimerization energy of neutral MB predicted by the force field (-46.31 kcal·mol^{-1}) is nearly double the value predicted by DFT (-24.35 kcal·mol^{-1}). Structural properties of MB$_2$ using either DFT or FF methods are in good agreement; the MB molecules are sandwiched to enhance hydrophobic ring−ring interactions, with the aromatic sulfur atom opposite the aromatic nitrogen atom in the adjacent molecule. More details of this structure will be discussed below with the results from the classical MD simulations.

As a separate validation of the DFT approach used here − particularly to examine the tendency of G06 dispersive corrections to overestimate interaction energies (Bučko *et al.*, 2013) − calculations of MB dimerization were also performed using two other methods: the B3LYP functional (Becke, 1993) with the same correction (sedc), and GGA/PBE with the

Table 2. Binding energies (kcal·mol^{-1}) for adsorption of neutral MB monomers and dimers, and MB$^+$ Cl$^-$ ion pairs on the siloxane surface of kaolinite.

Adsorbate	Orientation[a]	– Binding energy –	
		DFT	Classical
MB	parallel	– 24.82	– 21.35
MB$_2$	parallel	– 55.86	– 29.44
	perpendicular	– 14.50	– 23.63
MB$^+$ Cl$^-$	parallel[b]	– 142.53	– 126.44

[a] Orientation of MB or MB$_2$ relative to the siloxane surface.
[b] MB$^+$ adsorbed on the siloxane surface and Cl$^-$ adsorbed on the aluminol surface.

Tkatchenko-Scheffler (TS) method of incorporating van der Waals corrections (Tkatchenko and Scheffler, 2009). The B3LYP and TS methods result in dimerization energies of −51.78 kcal·mol^{-1} and −28.45 kcal·mol^{-1}, respectively. While dispersion correction greatly overestimates the B3LYP dimerization energy compared to the GGA/PBE methods, the use of the sedc model for dispersion corrections is equivalent to the parameter-free TS method.

Methylene blue binding energies on the siloxane surface of kaolinite (Table 2) reflect the energetically preferred adsorption to that surface compared to the gibbsite surface. For neutral monomers or dimers adsorbed with their molecular planes parallel to the siloxane surface, classical binding energies are slightly

weaker (more positive) than the corresponding DFT values, indicating that either the electrostatic or Lennard-Jones energy terms are relatively weak compared with DFT. The electrostatic interactions (*i.e.* partial charges) are unlikely to be too low, although other methods have been used to estimate partial charges of tetrahedral silicon and octahedral aluminum atoms in aluminosilicates that are significantly lower than those in *Clayff* (Heinz and Suter, 2004). Mulliken charge analyses of the DFT-optimized structures result in net charges of +0.08 e and +0.83 e for adsorbed MB and MB$^+$, respectively (adsorbed Cl$^-$ has a charge of −0.66 e). If anything, the electrostatic energies are too high based on the MB$^+$ net charge of +1.0 e used in the hybrid FF simulation. *Clayff* parameters can be modified to tune surface or interfacial properties for specific applications (Kerisit *et al.*, 2008; Ferrage *et al.*, 2011; Kerisit, 2011; Yu and Schmidt, 2011), but a transferrable method for doing this has yet to be implemented.

Geometry-optimized structures of MB monomers on the siloxane surface (Figure 2) indicate excellent agreement of structural properties between DFT and FF methods. Both MB and MB$^+$ adsorb with the molecular plane parallel to the siloxane surface. Optimized N−O and S−O distances in the FF-optimized structure deviate by at most 0.3 Å from the DFT result, and the near-planar orientation of methyl groups is similar. In the case of the MB$^+$ Cl$^-$ system, the chloride ion was placed near the aluminol surface for consistency
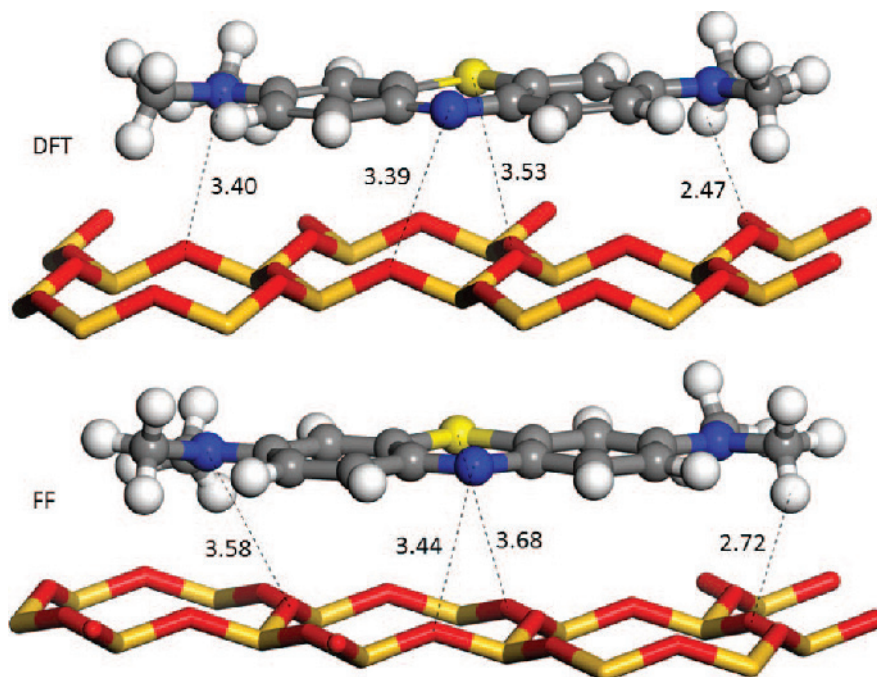

Figure 2. Geometry-optimized structures of a neutral MB monomer adsorbed on the siloxane surface of kaolinite from DFT and FF calculations. Average distances between MB atoms and surface oxygen atoms are indicated. The color scheme is the same as in Figure 1.

with previous MD (Vasconcelos *et al.*, 2007) and DFT (Geatches *et al.*, 2012) results showing preferred chloride ion adsorption to this surface. Larger electrostatic energies due to the presence of ions rather than a neutral molecule are reflected in the large binding energy of $MB^+ Cl^-$ compared to MB.

Geometry-optimized structures were also obtained for MB_2 dimers (Figure 3), where the MB monomers form a stack either parallel or perpendicular to the siloxane surface. The parallel orientation has a significantly stronger DFT binding energy (Table 2), while the classical binding energies are equivalent. For the perpendicular orientation (Figure 3), the $H-O_{surface}$ distances are similar for hydrogen atoms in methyl groups or aromatic rings. The DFT results show that forming an MB_2 dimer in parallel orientation is similar in energy to two separate MB monomers and enthalpically favorable compared to the MB_2 dimer in perpendicular orientation. The corresponding classical binding energies for MB_2 dimers do not match the DFT trends, indicating that the classical MB−MB interaction energies are too strong and the MB−kaolinite interactions are too weak.

Although the above comparisons highlight areas for improvement in interfacial mineral−organic force fields, some efforts have been made by Heinz and co-workers to develop a transferrable force field (INTERFACE FF) for such interfaces (Heinz *et al.*, 2013).

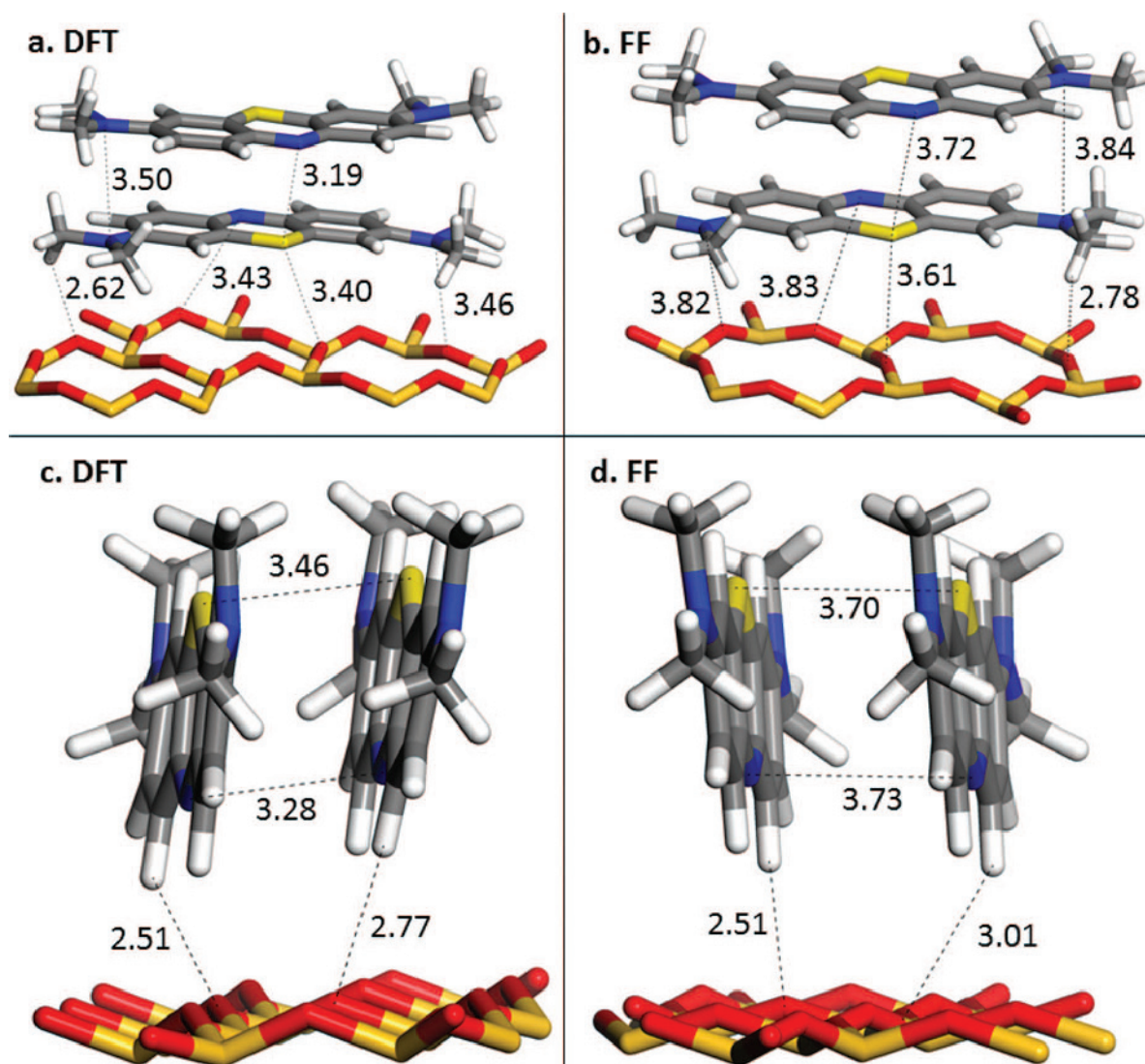The relatively good agreement in most structural and some energetic properties of adsorbed MB or MB^+

Figure 3. Geometry-optimized structures of neutral MB_2 dimers adsorbed on the siloxane surface of kaolinite from DFT and FF calculations. Numbers indicate average S−N and $H_{MB}-O_{surface}$ distances (Å) for hydrogen atoms in methyl groups and aromatic rings. The color scheme is the same as in Figure 1.

validate the following MD results of MB$^+$ in aqueous kaolinite pores. Classical MD simulations were used to examine the adsorption tendencies of MB, MB$^+$, and Cl$^-$ in an aqueous kaolinite pore. Both MB and MB$^+$ exhibit a clear preference for the siloxane surface, and both species form aggregates near the siloxane surface at concentrations above infinite dilution (Figure 4). Simulations were initiated with MB species placed near each surface and at the midplane of the pore, and in all cases MB$^+$ (and neutral MB) preferentially adsorbed at the siloxane surface. When present, chloride ions preferred the aluminol surface of kaolinite with little or no interaction with MB$^+$. The partitioning of MB$^+$ and Cl$^-$ in a kaolinite pore is consistent with the relative hydrophobicity of the siloxane surface compared to the aluminol surface. The adsorption of halide ions at the aluminol surface has been attributed to the slight localized positive charge on this surface (Vasconcelos *et al.*, 2007) as well as the formation of hydrogen bonds (Geatches *et al.*, 2012).

The adsorption of MB$^+$ onto the siloxane surface involves electrostatic as well as hydrophobic interactions. Similar to the gas-phase results (Figure 2), isolated MB$^+$ adsorbs parallel to the siloxane surface (Figure 4a) to maximize both hydrophobic interactions (MB$^+$ rings with siloxane rings) and electrostatic interactions (amine–surface and sulfur–surface). These MB$^+$–surface interactions are similar to *pi-pi* interactions that exist between aromatic molecules (Grimme, 2008) and between dye molecules and lignin (Perdih and Perdih, 2011). No attempt has been made to quantify the effect of methyl-group orientation because these rearrangements in general have a minor role in adsorption structure or energetics.

At higher concentrations, aggregates of adsorbed MB$^+$ consist mainly of MB$^+$ oriented perpendicular to the surface (Figure 4b), in agreement with MD simulations of MB$^+$ trimers and pentamers adsorbed on a dry mica surface (Yu *et al.*, 2003). Details of this surface structure will be explored in more detail below. This arrangement of MB$^+$ at the siloxane surface is a balance between electrostatic repulsion between adjacent ions and strong MB$^+$–MB$^+$ and MB$^+$–surface hydrophobic interactions. When the net charge is removed from each ion, neutral MB molecules prefer the siloxane surface as an amorphous aggregate with methyl groups directed toward the surface (Figure 4c). The effect of the delocalized +1 charge has a noticeable effect on adsorption structure, but hydrophobic MB–MB interactions play a key role regardless of MB charge.

One-dimensional atomic density profiles (Figure 5) serve to quantify the structure of adsorbed MB$^+$ on the kaolinite surface. At effectively infinite dilution, MB$^+$ maintains a consistent adsorption structure on the siloxane surface throughout the 5 ns production simulation (Figure 5a). Overlap of the aromatic N and S atoms indicates that MB$^+$ is oriented parallel to the surface. Based on the peak positions of the aromatic N
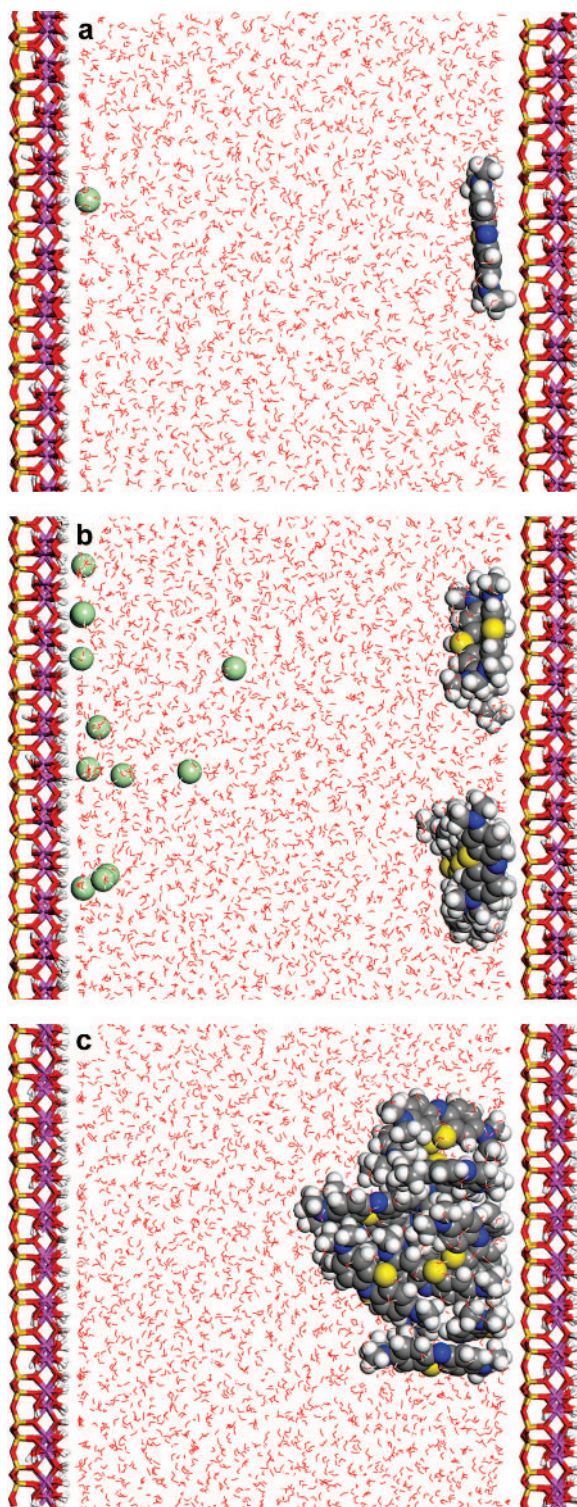

Figure 4. Equilibrium snapshots (*xz* plane) from MD simulations of MB in aqueous kaolinite pores: (a) 1 MB$^+$ Cl$^-$, (b) 12 MB$^+$ Cl$^-$, and (c) 14 neutral MB. The color scheme is the same as Figure 1, with the addition of Cl$^-$ (green).
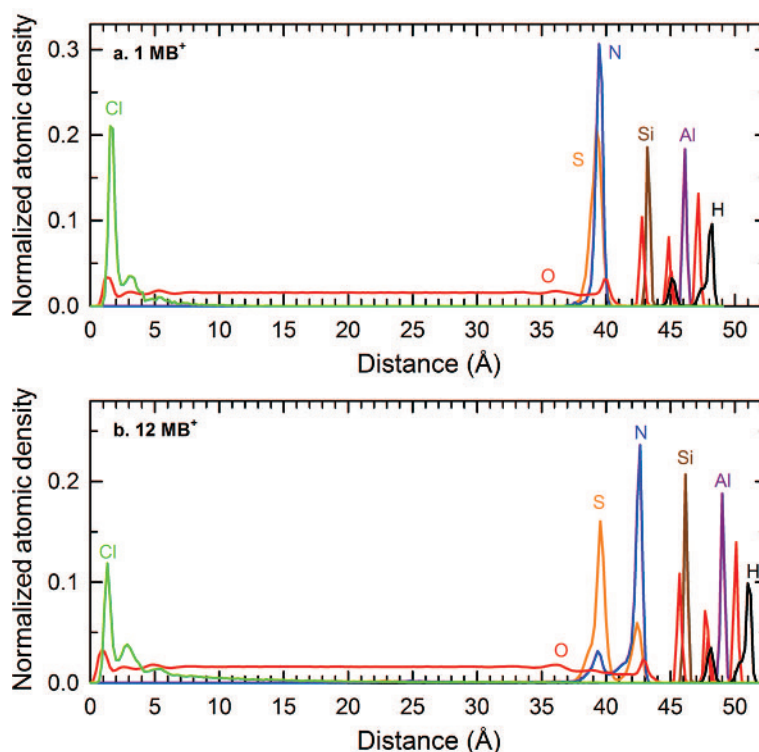
Figure 5. Atomic density profiles showing the structure of MB$^+$, Cl$^-$, and water adsorbed on the siloxane ($z \approx 50$ Å) or aluminol ($z \approx 0$ Å) surface of kaolinite. One-dimensional profiles show the structure of atoms in the aqueous kaolinite layers for the (a) 1 MB$^+$ Cl$^-$ and (b) 12 MB$^+$ Cl$^-$ systems. For MB$^+$, only nitrogen and sulfur atoms in the aromatic ring (N1, S1) are shown. For water, hydrogen atoms are omitted, and the density of oxygen atoms have been scaled for ease of viewing.

atoms and surface O atoms, the average distance between the MB plane and the siloxane surface is 3.1 Å, which is comparable to the interatomic distances reported for similar adsorption complexes (Figures 2, 3). As seen in the equilibrium snapshot (Figure 4a), the lone Cl$^-$ forms an inner-sphere surface complex coordinated by surface aluminol groups.

At the higher MB$^+$ concentration (12 MB$^+$ Cl$^-$), the MB$^+$ density profile suggests the presence of two molecular layers at the siloxane surface (Figure 5b). An equilibrium snapshot showing the siloxane surface (Figure 6) indicates only a monolayer of MB$^+$, however, arranged as a monomer, dimer, and a well-ordered one-dimensional (1D) chain. The local structure of the adsorbed dimer is similar to the gas-phase neutral dimer discussed previously, with sandwiched (MB$^+$)$_2$ perpendicular to the siloxane surface and oriented to enhance non-bonded S−N interactions. Interestingly, the average distance between aromatic nitrogen (N1) atoms and surface O atoms in the parallel dimer configuration (Figure 5b) is nearly identical to the planar configuration (Figure 5a). Because the dimer and the 1D chain both indicate the same arrangement of MB$^+$ perpendicular to the siloxane surface, similarly arranged trimers and higher associations of oligomers would be expected under different simulation conditions (e.g. system size, concentration, temperature, etc.).
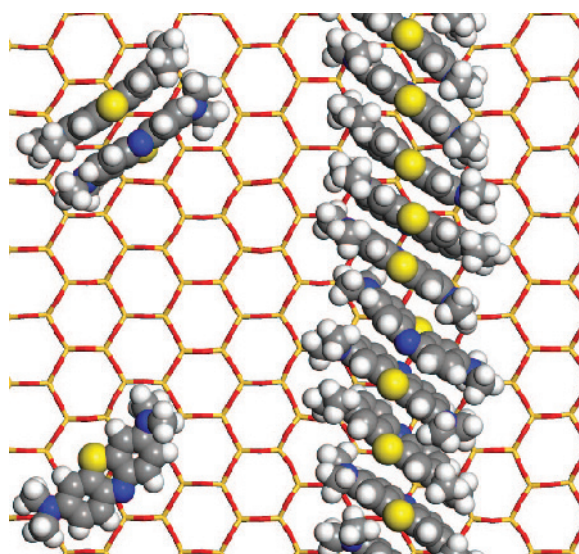

Figure 6. Equilibrium snapshot (xy plane) of 12 MB$^+$ Cl$^-$ in an aqueous kaolinite pore. The configuration is the same as in Figure 4b but with water molecules and chloride ions removed, and only the nearest siloxane surface shown for ease of viewing. The color scheme is the same as Figure 1.

Aggregation of MB^+ at this surface is consistent with spectroscopic results indicating the presence of dimers, trimers, and higher aggregates at smectite surfaces (Cenens and Schoonheydt, 1988; Schoonheydt and Heughebaert, 1992; Jacobs and Schoonheydt, 1999). The UV-Vis spectrum of MB^+ adsorbed on smectite surfaces has been shown to change over time to represent mostly adsorbed monomers (Jacobs and Schoonheydt, 2001). This behavior was not observed over the nanosecond scale of the simulations in part because the strong intermolecular MB^+–MB^+ interactions with the OPLS-based potential parameters reduce the likelihood of aggregate dissociation.

Orientation of MB^+ relative to the hydrated siloxane surface of kaolinite observed in the MD simulations have been quantified (Figure 7). An isolated MB^+ oriented parallel to the surface shows a slight preference for the S atom to tilt away from the surface ($\phi \approx 5°$) due to the steric hindrance of the amine groups. At higher concentrations ($12 \, MB^+ \, Cl^-$), there are three prevalent configurations: (1) MB^+ parallel to the surface with a slight preference for the S atom to tilt outward, as in the previous case ($\phi \approx 5°$, Figure 2), and perpendicular orientations with either (2) the aromatic S or (3) the aromatic N atom closest to the surface, corresponding to $\phi \approx -85°$ and $\phi \approx +85°$, respectively. Configuration (3) is the most probable alignment and dominates the structure in the 1D chain represented in Figure 6. Electrostatic repulsion due to the close proximity of adjacent S and N atoms is overcome by the much stronger hydrophobic interactions between aromatic rings.

The oxygen coordination environment near S and N atoms in isolated MB^+ in bulk solution (infinite dilution) is compared with a kaolinite inner-sphere surface
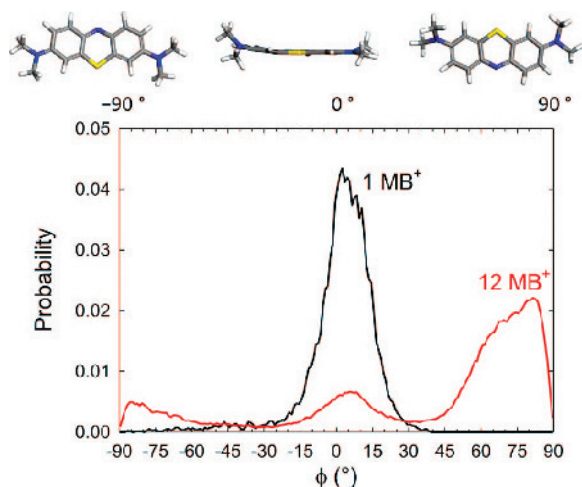
complex (Figure 8) using radial distribution functions (RDFs). The broad first peaks and large S–O and N1–O distances are indicative of weakly coordinated water molecules. For S and N atoms in the aromatic ring of MB^+, steric hindrance restricts the closest approach of

Figure 7. Orientation of adsorbed MB^+ relative to the hydrated kaolinite surface for $1 \, MB^+$ and $12 \, MB^+$, where ϕ is the angle formed between the S-N1 vector in MB^+ (aromatic ring S and N atoms) and the siloxane surface of kaolinite. Representative molecular models indicate the three predominant orientations.
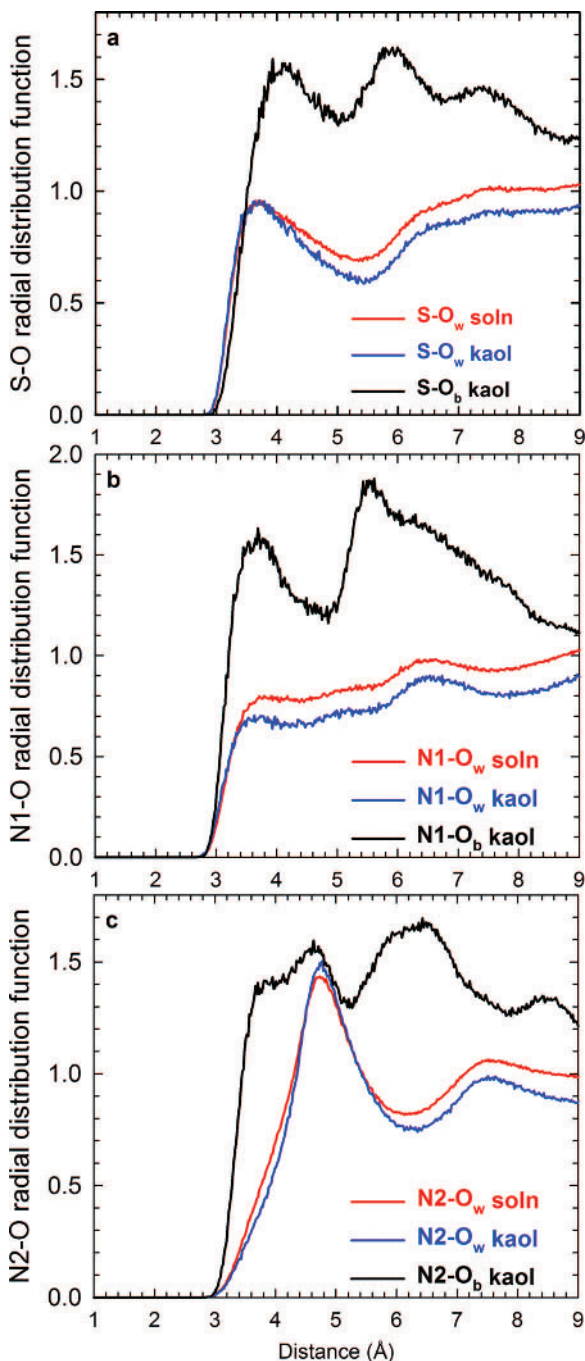

Figure 8. Sulfur-oxygen and nitrogen-oxygen radial distribution functions (RDFs) between the (a) sulfur, (b) aromatic nitrogen (N1), and (c) amine nitrogen (N2) atoms in MB^+ and H_2O in bulk solution (O_w soln), H_2O in the kaolinite pore (O_w kaol), and bridging oxygen atoms on the siloxane surface (O_b kaol).

water oxygen atoms to ~3.6 Å, much longer than the 2.0 Å distances observed in the hydration surface of aqueous SO_2 (Shamay *et al.*, 2013). The association of water molecules about the amine groups (N2) shows additional coordination structure due to hydrogen bonding interactions between water oxygen and amine hydrogen atoms.

Surface oxygen atoms of kaolinite also coordinate to adsorbed MB^+ (Figure 8), and again a different coordination environment for amine groups was observed compared to the sulfur and nitrogen atoms in the aromatic ring. The first peak of surface oxygen atoms about aromatic ring atoms is qualitatively similar to water oxygen atoms, with $S-O_b$ and $N1-O_b$ distances similar to $S-O_w$ and $N1-O_w$ distances (O_b and O_w refer to bridging surface oxygen and water oxygen atoms, respectively). Amine groups near the siloxane surface are characterized by the $N2-O_b$ peak at 3.7 Å, which is consistent with coordination about the aromatic nitrogen. The second $N2-O_b$ peak at 4.7 Å is consistent with the first peak seen in the $N2-O_w$ distributions. S-O and N-O coordination numbers for first-shell interactions have been determined (Table 3). For the inner-sphere complex, the first coordination shell consists of both water oxygen atoms and surface oxygen atoms, with the sum of these coordination numbers for adsorbed MB^+ nearly identical to those observed for MB^+ in an aqueous solution.

Hydration and adsorption enthalpies of MB^+ Cl^- from MD simulations in bulk solution and kaolinite pores were calculated from average potential energies of the hydrated or adsorbed model system and the sum of average potential energies of the isolated species (gas-phase MB^+ or Cl^-, bulk water, or water-filled kaolinite pore). The change in volume upon hydration or adsorption is assumed to be negligible. The adsorption enthalpy of MB^+ Cl^- in the kaolinite pore is -112.7 kcal·mol^{-1}, which is only slightly more favorable than the sum of hydration enthalpies for isolated MB^+ (-18.7 kcal·mol^{-1}) and Cl^- (-80.5 kcal·mol^{-1}) ions. This adsorption enthalpy is similar in magnitude to the corresponding 0 K gas-phase binding energy (-126.4 kcal·mol^{-1}, Table 2). The adsorption of MB^+ at an aqueous mineral surface will be accompanied by

significant rearrangement of water molecules, so the accompanying entropy changes may significantly alter the free energy of adsorption.

CONCLUSIONS

The original aim of this study was two-fold. The first was to use molecular simulation to address unresolved issues related to the adsorption of organic dyes on mineral surfaces. Kaolinite was chosen to represent neutral siloxane and gibbsite-like $Al(OH)_3$ surfaces that will form a baseline for comparison with charged surfaces (future work). The use of organic dyes to characterize clays and other minerals highlights the importance of a detailed understanding of the adsorption process. The second aim was to shed light on the common practice of combining independently developed force fields for molecular simulations of hybrid mineral–organic systems. Comparison of FF results with DFT results provides the best available structural and energetic properties for further development of hybrid force fields. Some degree of confidence can be placed in the DFT results because of the high level of theory − including dispersion interactions − used to perform electronic structure calculations on a large periodic model.

Although the FF-predicted structural properties of adsorbed monomers and dimers show good agreement with the corresponding DFT results, differences in adsorption energies point to areas of improvement. The FF-predicted gas-phase binding energies are consistently lower (and weaker) than the corresponding quantum values, while the classical gas-phase dimerization energy is nearly double the DFT value. If these results prove to be consistent with similar studies of mineral–organic interfaces, it appears that subsequent force field development should result in stronger mineral–organic (and possibly water–organic) interactions and weaker organic–organic interactions. Tuning the mineral–organic interactions is of much greater interest because some general FFs predict accurately condensed phase properties of organics (Jorgensen *et al.*, 1996). The failure of the OPLS-based parameters to predict the DFT dimerization energy may be a special case because this molecule has some unique features that are well beyond the training set of molecules used to develop OPLS. Instead of relying on the transferability of FF parameters, deriving intermolecular FF parameters from a first-principles approach has already been demonstrated using, for example, symmetry-adapted perturbation theory (Dehez *et al.*, 2007; Totton *et al.*, 2010; Tafipolsky and Engels, 2011; McDaniel and Schmidt, 2013).

The present study demonstrates the need for further molecular analysis of complex organoclay systems such as the MB−kaolinite association. Kaolinite, categorized as an uncharged clay mineral and typically not having

Table 3. Coordination numbers of S−O and N−O interactions between MB^+ and first-shell oxygen atoms in aqueous solution and adsorbed to the siloxane surface of kaolinite[a].

MB^+ atom	Aqueous solution	Kaolinite pore	
		O_w	O_b
S	13.7	8.4	5.1
N1 (aromatic)	8.6	5.2	4.7
N2 (amine)	25.5	16.9	6.6

[a] Coordination numbers were calculated at the minimum of the first RDF peak except for $N2-O_b$, when the second peak was used.

adsorbed interlayer species, provides a relatively simple endmember case. More complex organoclay systems, involving smectites (*e.g.* montmorillonite and beidellite), have greater ability to adsorb organic dyes and potentially develop intercalated and/or ion-exchanged organic structures. As a practical example, the adsorption of MB has been considered for the simultaneous determination of both surface area and cation exchange capacity of smectites (Yukselen-Aksoy and Kaya, 2008; Yener *et al.*, 2012). To date, very limited effort has been made to explore the molecular mechanisms that control organic−clay structure and dynamics. Moreover, it would be beneficial to expand these approaches to improve the link between molecular simulation and spectroscopy, especially in the interpretation of UV-Vis spectra of organoclay systems. An investigation of electronic transitions associated with MB using open-shell DFT methods can determine the energy shifts of the electron relaxation from excited states as impacted by the configuration of MB (monomer, dimer, or larger aggregate) and by the adsorbed structure of the MB on a particular kaolinite surface.

REFERENCES

Avena, M.J., Valenti, L.E., Pfaffen, V., and De Pauli, C.P. (2001) Methylene blue dimerization does not interfere in surface-area measurements of kaolinite and soils. *Clays and Clay Minerals*, **49**, 168−173.

Becke, A.D. (1993) Density-functional thermochemistry. III. The role of exact exchange. *The Journal of Chemical Physics*, **98**, 5648−5652.

Bish, D.L. (1993) Rietveld refinement of the kaolinite structure at 1.5 K. *Clays and Clay Minerals*, **41**, 738−744.

Brindley, G.W. and Thompson, T.D. (1970) Methylene blue absorption by montmorillonites. Determinations of surface areas and exchange capacities with different initial cation saturations (clay-organic studies XIX). *Israel Journal of Chemistry*, **8**, 409−415.

Bučko, T., Lebègue, S., Hafner, J., and Ángyán, J.G. (2013) Tkatchenko-Scheffler van der Waals correction method with and without self-consistent screening applied to solids. *Physical Review B*, **87**, 064110.

Bujdak, J., Iyi, N., Kaneko, Y., and Sasai, R. (2003) Molecular orientation of methylene blue cations adsorbed on clay surfaces. *Clay Minerals*, **38**, 561−572.

Čapková, P., Malý, P., Pospíšil, M., Klika, Z., Weissmannová, H., and Weiss, Z. (2004) Effect of surface and interlayer structure on the fluorescence of rhodamine b-montmorillonite: Modeling and experiment. *Journal of Colloid and Interface Science*, **277**, 128−137.

Cenens, J. and Schoonheydt, R.A. (1988) Visible spectroscopy of methylene-blue on hectorite, Laponite-b, and barasym in aqueous suspension. *Clays and Clay Minerals*, **36**, 214−224.

Chagovets, V.V., Kosevich, M.V., Stepanian, S.G., Boryak, O.A., Shelkovsky, V.S., Orlov, V.V., Leontiev, V.S., Pokrovskiy, V.A., Adamowicz, L., and Karachevtsev, V.A. (2012) Noncovalent interaction of methylene blue with carbon nanotubes: Theoretical and mass spectrometry characterization. *Journal of Physical Chemistry C*, **116**, 20579−20590.

Clark, S.J., Segall, M.D., Pickard, C.J., Hasnip, P.J., Probert, M.J., Refson, K., and Payne, M.C. (2005) First principles methods using CASTEP. *Zeitschrift Fur Kristallographie*, **220**, 567−570.

Croteau, T., Bertram, A.K., and Patey, G.N. (2008) Adsorption and structure of water on kaolinite surfaces: Possible insight into ice nucleation from grand canonical Monte Carlo calculations. *Journal of Physical Chemistry A*, **112**, 10708−10712.

Croteau, T., Bertram, A.K., and Patey, G.N. (2009) Simulation of water adsorption on kaolinite under atmospheric conditions. *Journal of Physical Chemistry A*, **113**, 7826−7833.

Cygan, R.T., Liang, J.-J., and Kalinichev, A.G. (2004) Molecular models of hydroxide, oxyhydroxide, and clay phases and the development of a general force field. *Journal of Physical Chemistry B*, **108**, 1255−1266.

Dehez, F., Angyan, J.G., Gutierrez, I.S., Luque, F.J., Schulten, K., and Chipot, C. (2007) Modeling induction phenomena in intermolecular interactions with an ab initio force field. *Journal of Chemical Theory and Computation*, **3**, 1914−1926.

Demichelis, R., Civalleri, B., Ferrabone, M., and Dovesi, R. (2010) On the performance of eleven DFT functionals in the description of the vibrational properties of aluminosilicates. *International Journal of Quantum Chemistry*, **110**, 406−415.

Enescu, M., Ridard, J., Gheorghe, V., and Levy, B. (2002) Electron transfer modeling in condensed phase by molecular dynamics simulation: Application to methylene blue-guanine complex in water. *The Journal of Physical Chemistry B*, **106**, 176−184.

Fafard, J., Lyubimova, O., Stoyanov, S.R., Dedzo, G.K., Gusarov, S., Kovalenko, A., and Detellier, C. (2013) Adsorption of indole on kaolinite in nonaqueous media: Organoclay preparation and characterization, and 3D-RISM-KH molecular theory of solvation investigation. *Journal of Physical Chemistry C*, **117**, 18556−18566.

Ferrage, E., Sakharov, B.A., Michot, L.J., Delville, A., Bauer, A., Lanson, B., Grangeon, S., Frapper, G., Jiménez-Ruiz, M., and Cuello, G.J. (2011) Hydration properties and interlayer organization of water and ions in synthetic Na-smectite with tetrahedral layer charge. Part 2. Toward a precise coupling between molecular simulations and diffraction data. *The Journal of Physical Chemistry C*, **115**, 1867−1881.

Geatches, D.L., Jacquet, A., Clark, S.J., and Greenwell, H.C. (2012) Monomer adsorption on kaolinite: Modeling the essential ingredients. *Journal of Physical Chemistry C*, **116**, 22365−22374.

Ghosh, D. and Bhattacharyya, K.G. (2002) Adsorption of methylene blue on kaolinite. *Applied Clay Science*, **20**, 295−300.

Grimme, S. (2006) Semiempirical GGA-type density functional constructed with a long-range dispersion correction.

Journal of Computational Chemistry, **27**, 1787−1799.

Grimme, S. (2008) Do special noncovalent pi-pi stacking interactions really exist? *Angewandte Chemie-International Edition*, **47**, 3430−3434.

Hang, P.T. and Brindley, G.W. (1970) Methylene blue absorption by clay minerals. Determination of surface areas and cation exchange capacities (clay-organic studies XVIII). *Clays and Clay Minerals*, **18**, 203−212.

Haria, N.R., Grest, G.S., and Lorenz, C.D. (2013) Viscosity of nanoconfined water between hydroxyl basal surfaces of kaolinite: Classical simulation results. *Journal of Physical Chemistry C*, **117**, 6096−6104.

Headen, T.F. and Boek, E.S. (2011) Potential of mean force calculation from molecular dynamics simulation of asphaltene molecules on a calcite surface. *Energy & Fuels*, **25**, 499−502.

Heinz, H. and Suter, U.W. (2004) Atomic charges for classical simulations of polar systems. *Journal of Physical Chemistry B*, **108**, 18341−18352.

Heinz, H., Lin, T.J., Mishra, R.K., and Emami, F.S. (2013) Thermodynamically consistent force fields for the assembly of inorganic, organic, and biological nanostructures: The INTERFACE force field. *Langmuir*, **29**, 1754−1765.

Heister, K. (2014) The measurement of the specific surface area of soils by gas and polar liquid adsorption methods − limitations and potentials. *Geoderma*, **216**, 75−87.

Homem-de-Mello, P., Mennucci, B., Tomasi, J., and da Silva, A.B.F. (2005) The effects of solvation in the theoretical spectra of cationic dyes. *Theoretical Chemistry Accounts*, **113**, 274−280.

Hou, X.J., Li, H.Q., Li, S.P., and He, P. (2014) Theoretical study of the intercalation behavior of ethylene glycol on kaolinite. *Journal of Physical Chemistry C*, **118**, 26017−26026.

Jacobs, K.Y. and Schoonheydt, R.A. (1999) Spectroscopy of methylene blue-smectite suspensions. *Journal of Colloid and Interface Science*, **220**, 103−111.

Jacobs, K.Y. and Schoonheydt, R.A. (2001) Time dependence of the spectra of methylene blue-clay mineral suspensions. *Langmuir*, **17**, 5150−5155.

Johnston, K. (2014) A van der Waals density functional study of the adsorption of ethanol on the alpha-alumina (0001) surface. *Surface Science*, **621**, 16−22.

Jorgensen, W.L., Madura, J.D., and Swenson, C.J. (1984) Optimized intermolecular potential functions for liquid hydrocarbons. *Journal of the American Chemical Society*, **106**, 6638−6646.

Jorgensen, W.L. and Severance, D.L. (1990) Aromatic−aromatic interactions − free-energy profiles for the benzene dimer in water, chloroform, and liquid benzene. *Journal of the American Chemical Society*, **112**, 4768−4774.

Jorgensen, W.L. and Tirado-Rives, J. (1988) The OPLS potential functions for proteins. Energy minimizations for crystals of cyclic peptides and crambin. *Journal of the American Chemical Society*, **110**, 1657−1666.

Jorgensen, W.L., Maxwell, D.S., and Tirado-Rives, J. (1996) Development and testing of the OPLS all-atom force field on conformational energetics and properties of organic liquids. *Journal of the American Chemical Society*, **118**, 11225−11236.

Kerisit, S. (2011) Water structure at hematite−water interfaces. *Geochimica et Cosmochimica Acta*, **75**, 2043−2061.

Kerisit, S., Liu, C., and Ilton, E.S. (2008) Molecular dynamics simulations of the orthoclase (001)- and (010)-water interfaces. *Geochimica et Cosmochimica Acta*, **72**, 1481−1497.

Klebow, B. and Meleshyn, A. (2011) Aggregation of alkyltrimethylammonium ions at the cleaved muscovite mica-water interface: A Monte Carlo study. *Langmuir*, **27**, 12968−12976.

Klika, Z., Weissmannova, H., Čapková, P., and Pospíšil, M. (2004) The rhodamine b intercalation of montmorillonite. *Journal of Colloid and Interface Science*, **275**, 243−250.

Klika, Z., Čapková, P., Horáková, P., Valášková, M., Malý, P., Macháň, R., and Pospíšil, M. (2007) Composition, structure, and luminescence of montmorillonites saturated with different aggregates of methylene blue. *Journal of Colloid and Interface Science*, **311**, 14−23.

Klika, Z., Pustkova, P., Praus, P., Kovar, P., Pospíšil, M., Malý, P., Grygar, T., Kulhankova, L., and Čapková, P. (2009) Fluorescence of reduced charge montmorillonite complexes with methylene blue: Experiments and molecular modeling. *Journal of Colloid and Interface Science*, **339**, 416−423.

Kohn, W. and Sham, L.J. (1965a) Quantum density oscillations in an inhomogeneous electron gas. *Physical Review*, **137**, 1697−1705.

Kohn, W. and Sham, L.J. (1965b) Self-consistent equations including exchange and correlation effects. *Physical Review*, **140**, 1133−1138.

Kovar, P., Pospíšil, M., Malý, P., Klika, Z., Čapková, P., Horáková, P., and Valáškova, M. (2009) Molecular modeling of surface modification of Wyoming and Cheto montmorillonite by methylene blue. *Journal of Molecular Modeling*, **15**, 1391−1396.

Kresse, G. and Furthmuller, J. (1996) Efficient iterative schemes for ab initio total-energy calculations using a plane-wave basis set. *Physical Review B*, **54**, 11,169−11,186.

Lagaly, G., Ogawa, M., and Dekany, I. (2013) Clay mineral-organic interactions. Pp. 309−377 in: *Handbook of Clay Science*, 2nd edition (F. Bergaya, and G. Lagaly, editors). Elsevier, Amsterdam.

Levy, B. and Enescu, M. (1998) Theoretical study of methylene blue: A new method to determine partial atomic charges; investigation of the interaction with guanine. *Journal of Molecular Structure:THEOCHEM*, **432**, 235−245.

Lofaj, M. and Bujdak, J. (2012) Detection of smectites in ppm and sub-ppm concentrations using dye molecule sensors. *Physics and Chemistry of Minerals*, **39**, 227−237.

Maček, M., Mauko, A., Madenovič, A., Majes, B., and Petkovšek, A. (2013) A comparison of methods used to characterize the soil-specific surface area of clays. *Applied Clay Science*, **83−84**, 144−152.

McDaniel, J.G. and Schmidt, J.R. (2013) Physically motivated force fields from symmetry-adapted perturbation theory. *The Journal of Physical Chemistry A*, **117**, 2053−2066.

McNellis, E.R., Meyer, J., and Reuter, K. (2009) Azobenzene at coinage metal surfaces: Role of dispersive van der Waals interactions. *Physical Review B*, **80**, 205414.

Monkhorst, H.J. and Pack, J.D. (1976) Special points for Brillouin-zone integrations. *Physical Review B*, **13**, 5188−5192.

Neumann, M.G., Gessner, F., Schmitt, C.C., and Sartori, R. (2002) Influence of the layer charge and clay particle size on the interactions between the cationic dye methylene blue and clays in an aqueous suspension. *Journal of Colloid and Interface Science*, **255**, 254−259.

Oz, M., Lorke, D.E., Hasan, M., and Petroianu, G.A. (2011) Cellular and molecular actions of methylene blue in the nervous system. *Medicinal Research Reviews*, **31**, 93−117.

Payne, M.C., Teter, M.P., Allan, D.C., Arias, T.A., and Joannopoulos, J.D. (1992) Iterative minimization techniques for *ab initio* total-energy calculations: Molecular dynamics and conjugate gradients. *Reviews in Modern Physics*, **64**, 1045−1097.

Perdew, J.P., Burke, K., and Ernzerhof, M. (1996) Generalized

gradient approximation made simple. *Physical Review Letters*, **77**, 3865−3868.

Perdih, F. and Perdih, A. (2011) Lignin selective dyes: Quantum-mechanical study of their characteristics. *Cellulose*, **18**, 1139−1150.

Pfrommer, B.G., Cote, M., Louie, S.G., and Cohen, M.L. (1997) Relaxation of crystals with the quasi-Newton method. *Journal of Computational Physics*, **131**, 233−240.

Plimpton, S.J., Pollock, R., and Stevens, M. (1997) Particle-mesh Ewald and rRESPA for parallel molecular dynamics simulations. Eighth SIAM Conference on Parallel Processing for Scientific Computing, Minneapolis, Minnesota, USA.

Praus, P., Veteška, M., and Pospíšil, M. (2011) Adsorption of phenol and aniline on natural and organically modified montmorillonite: Experiment and molecular modelling. *Molecular Simulation*, **37**, 964−974.

Quintao, A.D., Coutinho, K., and Canuto, S. (2002) Theoretical study of the hydrogen bond interaction between methylene blue and water and possible role on energy transfer for photodynamics. *International Journal of Quantum Chemistry*, **90**, 634−640.

Rai, B., Sathish, P., Tanwar, J., Pradip, Moon, K.S., and Fuerstenau, D.W. (2011) A molecular dynamics study of the interaction of oleate and dodecylammonium chloride surfactants with complex aluminosilicate minerals. *Journal of Colloid and Interface Science*, **362**, 510−516.

Rytwo, G., Nir, S., and Margulies, L. (1995) Interactions of monovalent organic cations with montmorillonite: Adsorption studies and model calculations. *Soil Science Society of America Journal*, **59**, 554−564.

Schoonheydt, R.A. and Heughebaert, L. (1992) Clay adsorbed dyes − methylene-blue on Laponite. *Clay Minerals*, **27**, 91−100.

Shamay, E.S., Valley, N.A., Moore, F.G., and Richmond, G.L. (2013) Staying hydrated: The molecular journey of gaseous sulfur dioxide to a water surface. *Physical Chemistry Chemical Physics*, **15**, 6893−6902.

Smith, D.R. and Dang, L.X. (1994) Computer simulations of NaCl association in polarizable water. *Journal of Chemical Physics*, **100**, 3757−3766.

Tafipolsky, M. and Engels, B. (2011) Accurate intermolecular potentials with physically grounded electrostatics. *Journal of Chemical Theory and Computation*, **7**, 1791−1803.

Teleman, O., Jonsson, B., and Engstrom, S. (1987) A molecular dynamics simulation of a water model with intramolecular degrees of freedom. *Molecular Physics*, **60**, 193−203.

Tenney, C.M. and Cygan, R.T. (2014) Molecular simulation of carbon dioxide, brine, and clay mineral interactions and determination of contact angles. *Environmental Science & Technology*, **48**, 2035−2042.

Tkatchenko, A. and Scheffler, M. (2009) Accurate molecular van der Waals interactions from ground-state electron density and free-atom reference data. *Physical Review Letters*, **102**, 073005.

Tokarsky, J., Čapková, P., and Burda, J.V. (2012) Structure and stability of kaolinite/TiO_2 nanocomposite: DFT and MM computations. *Journal of Molecular Modeling*, **18**, 2689−2698.

Toth, R., Santese, F., Pereira, S.P., Nieto, D.R., Pricl, S.,

Fermeglia, M., and Posocco, P. (2012) Size and shape matter! A multiscale molecular simulation approach to polymer nanocomposites. *Journal of Materials Chemistry*, **22**, 5398−5409.

Totton, T.S., Misquitta, A.J., and Kraft, M. (2010) A first principles development of a general anisotropic potential for polycyclic aromatic hydrocarbons. *Journal of Chemical Theory and Computation*, **6**, 683−695.

Tunega, D., Bučko, T., and Zaoui, A. (2012) Assessment of ten DFT methods in predicting structures of sheet silicates: Importance of dispersion corrections. *Journal of Chemical Physics*, **137**, 114105.

Vanderbilt, D. (1990) Soft self-consistent pseudopotentials in a generalized eigenvalue formalism. *Physical Review B*, **41**, 7892−7895.

Vasconcelos, I.F., Bunker, B.A., and Cygan, R.T. (2007) Molecular dynamics modeling of ion adsorption to the basal surfaces of kaolinite. *Journal of Physical Chemistry C*, **111**, 6753−6762.

Wainwright, M. (2000) Methylene blue derivatives – suitable photoantimicrobials for blood product disinfection? *International Journal of Antimicrobial Agents*, **16**, 381−394.

Wainwright, M. and Crossley, K.B. (2002) Methylene blue – a therapeutic dye for all seasons? *Journal of Chemotherapy*, **14**, 431−443.

Wilson, N. and Muscat, J. (2002) The calculation of structural, elastic and phase stability properties of minerals using first principles techniques: A comparison of HF, DFT and hybrid functional treatments of exchange and correlation. *Molecular Simulation*, **28**, 903−915.

Yener, N., Bicer, C., Onal, M., and Sarikaya, Y. (2012) Simultaneous determination of cation exchange capacity and surface area of acid activated bentonite powders by methylene blue sorption. *Applied Surface Science*, **258**, 2534−2539.

Yu, K.A. and Schmidt, J.R. (2011) Elucidating the crystal face- and hydration-dependent catalytic activity of hydrotalcites in biodiesel production. *Journal of Physical Chemistry C*, **115**, 1887−1898.

Yu, C.-H., Newton, S.Q., Norman, M.A., Miller, D.M., Schafer, L., and Teppen, B.J. (2000) Molecular dynamics simulations of the adsorption of methylene blue at clay mineral surfaces. *Clays and Clay Minerals*, **48**, 665−681.

Yu, C.H., Newton, S.Q., Norman, M.A., Schafer, L., and Miller, D.M. (2003) Molecular dynamics simulations of adsorption of organic compounds at the clay mineral/ aqueous solution interface. *Structural Chemistry*, **14**, 175−185.

Yukselen-Aksoy, Y. and Kaya, A. (2008) Suitability of the methylene blue test for surface area, cation exchange capacity and swell potential determination of clayey soils. *Engineering Geology*, **102**, 38−45.

Zeitler, T.R., Greathouse, J.A., and Cygan, R.T. (2012) Effects of thermodynamic ensembles and mineral surfaces on interfacial water structure. *Physical Chemistry Chemical Physics*, **14**, 1728−1734.